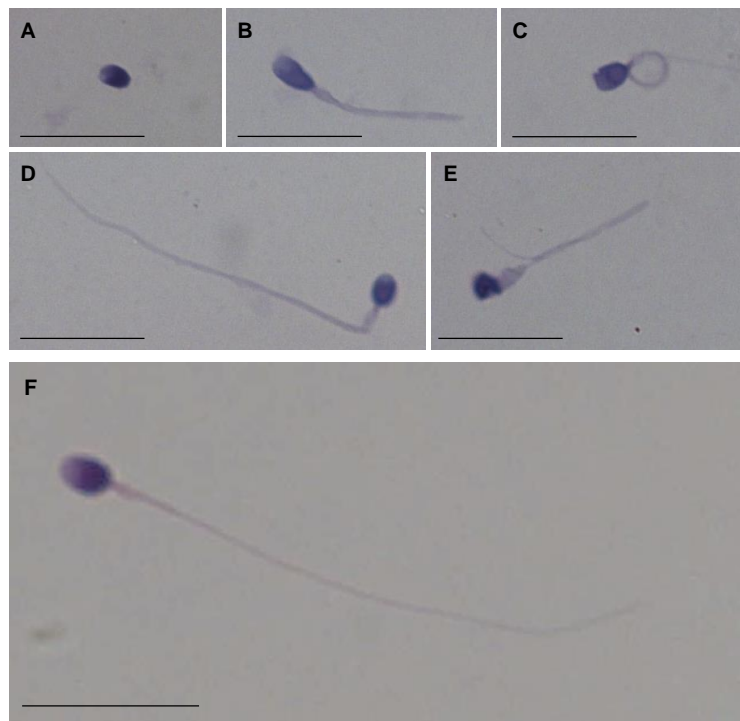


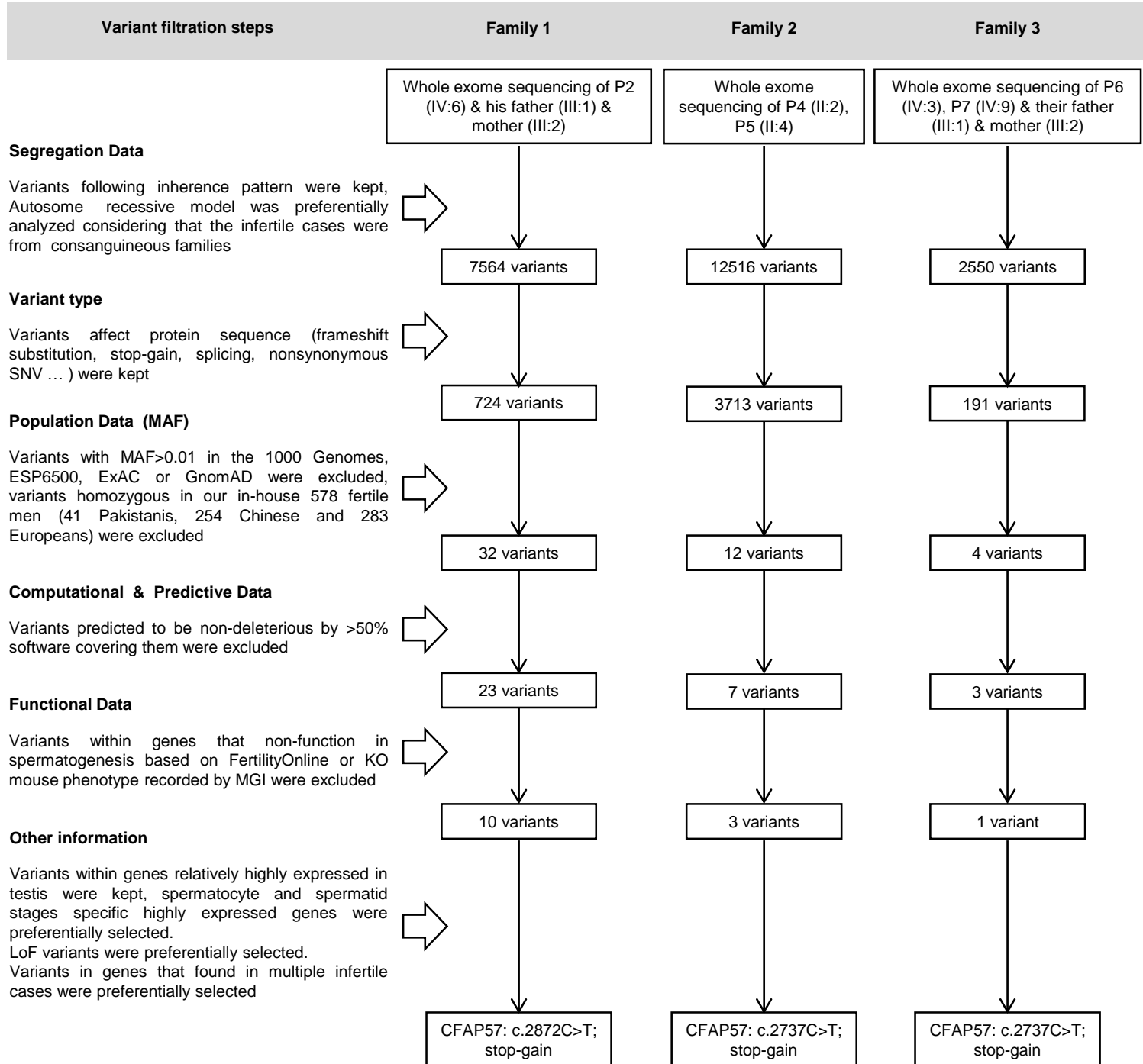
Supplementary Figure 1



Supplementary Figure 1. Sperm morphology of P7 and a fertile control. (A-E) Representative images showing spermatozoa with absent (A), short (B), coiled (C) and bent (D) flagella and flagella of irregular caliber (E) from P7 and spermatozoa with normal flagella (F) from a fertile control. Scale bars represent 10 μ m.

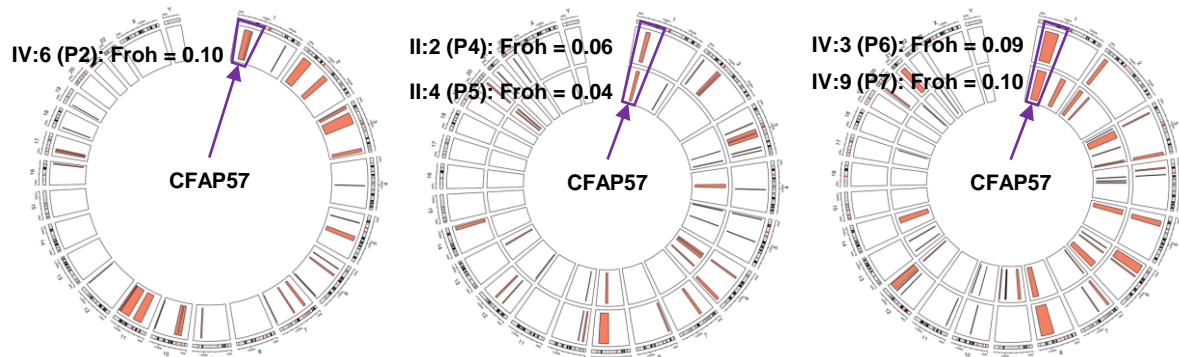
Supplementary Figure 2

A



B

CFAP57 variants following Autosome recessive models are within Regions of Homozygosity (RoHs) in infertile cases

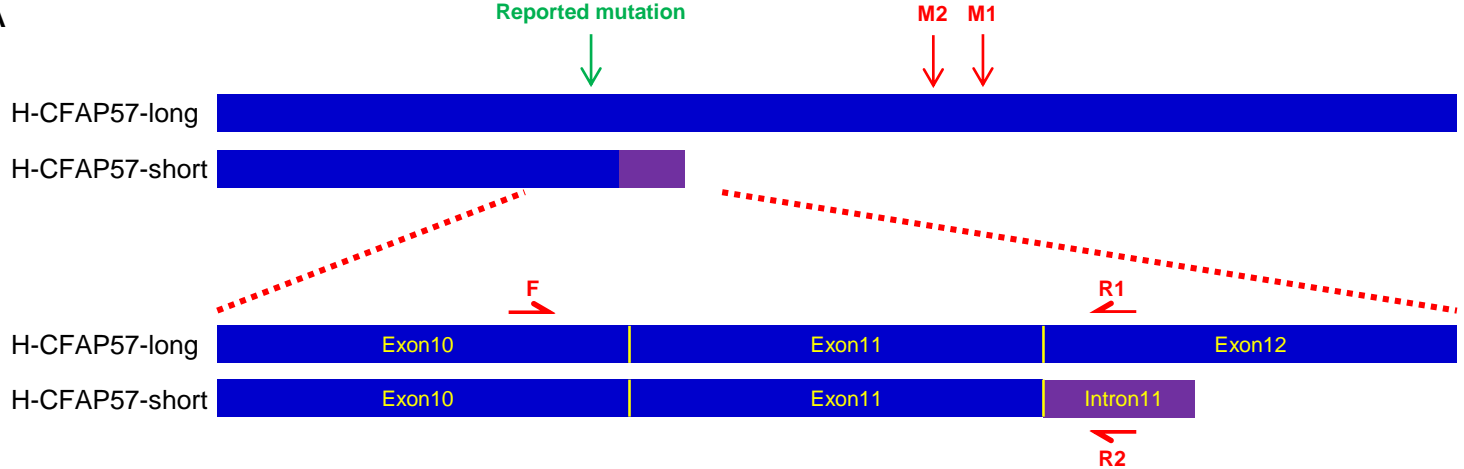


Supplementary Figure 2. Bioinformatic analysis of candidate variants. (A) Candidate pathogenic variants were filtered.

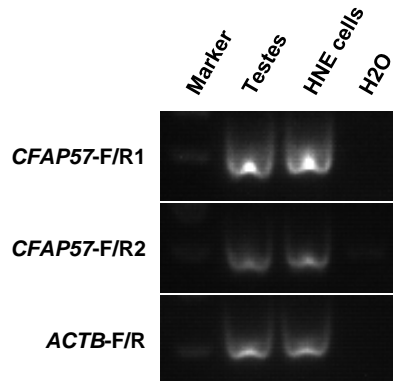
(B) CFAP57 variants are within RoHs in infertile cases.

Supplementary Figure 3

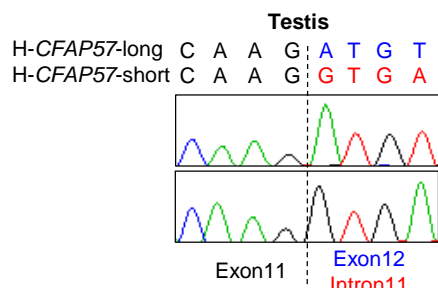
A



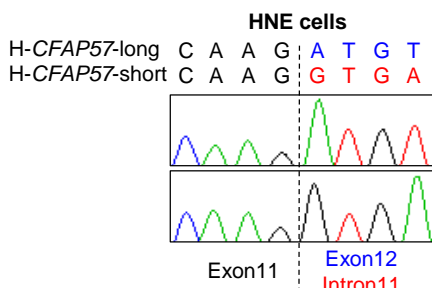
B



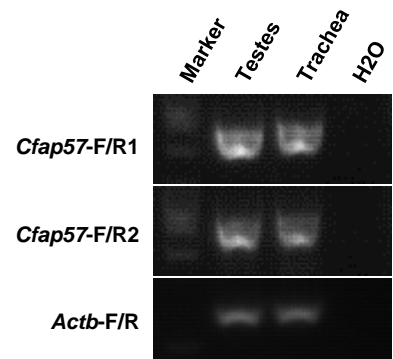
C



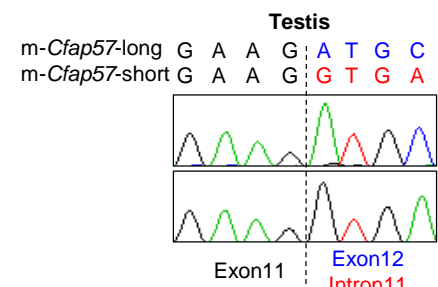
D



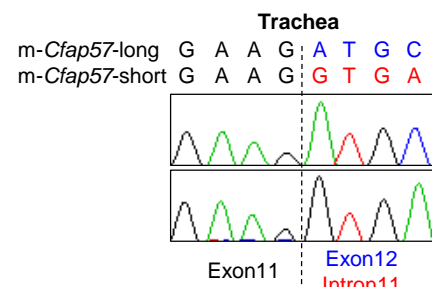
E



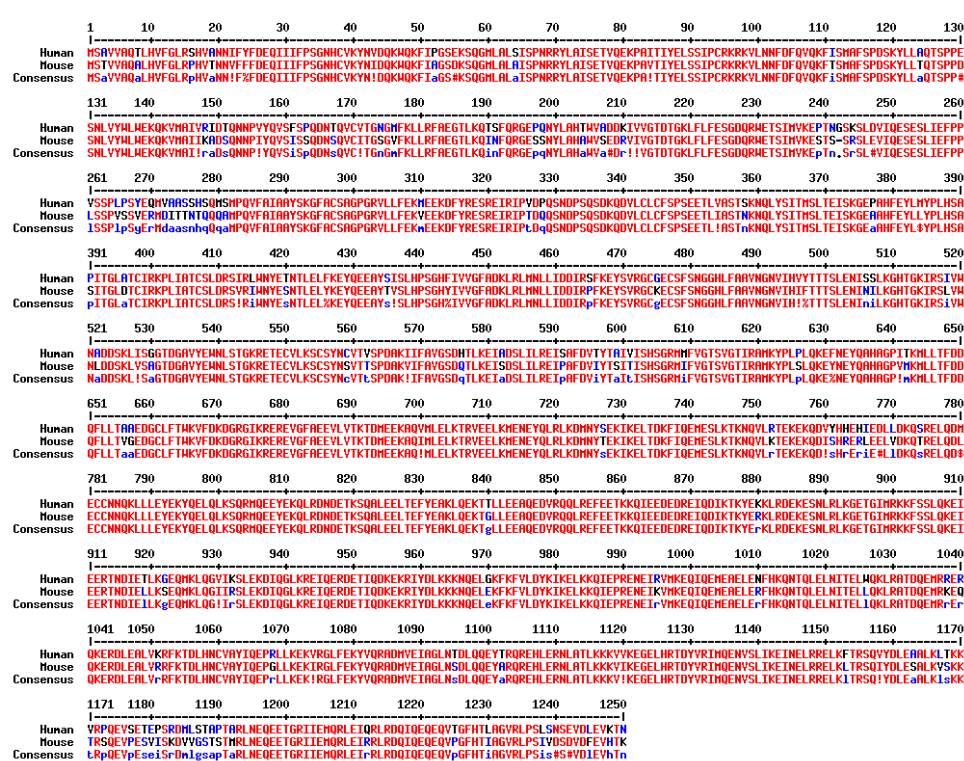
F



G

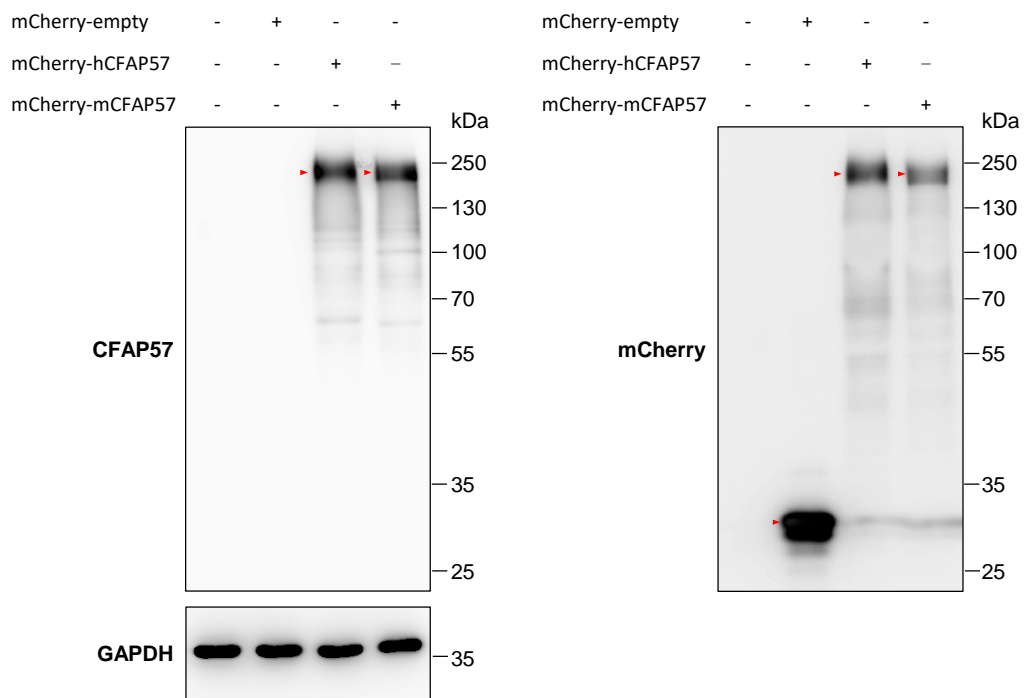


H



Supplementary Figure 3. Two transcripts of *CFAP57/Cfap57* are both expressed in testes and HNE cells/ mice trachea. (A) Schematic illustrating two transcriptions of *CFAP57*. (B-D) PAGE and Sanger sequencing results showing the expression of both *CFAP57* transcriptions in testes and HNE cells. (E-G) PAGE and Sanger sequencing results showing the expression of both *Cfap57* transcriptions in testes and trachea. (H) *CFAP57* was conserved in human and mice. Sequence alignment shows conservation of human and mice *CFAP57* protein. Red letters represent completely same sequence. The alignment was performed using the online software MultAlin (<http://multalin.toulouse.inra.fr/multalin/multalin.html>).

Supplementary Figure 4

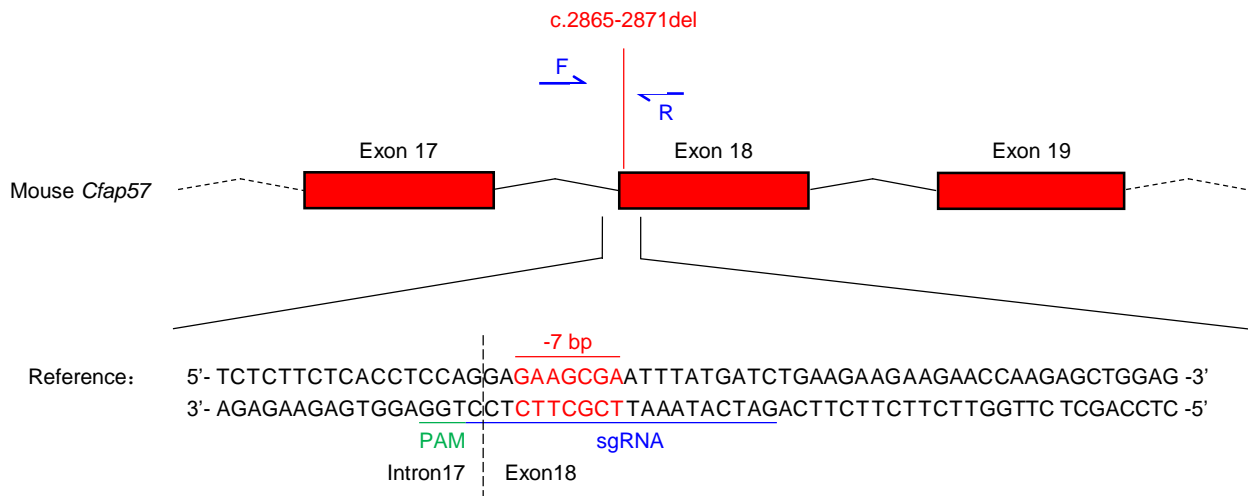


Supplementary Figure 4. Anti-CFAP57 antibody was able to recognize both human and mice CFAP57 *in vitro*.

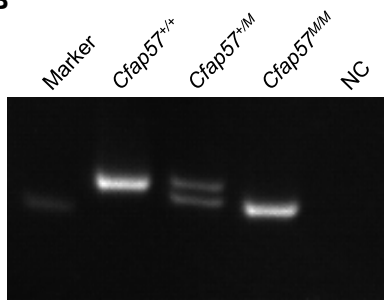
MCherry-tagged human and mice CFAP57 and mCherry were expressed in cultured HEK293T cells. Both anti-mCherry antibodies and anti-CFAP57 antibodies were used to detect the mCherry-tagged CFAP57. Arrows indicate the positions of bands corresponding to proteins of interest.

Supplementary Figure 5

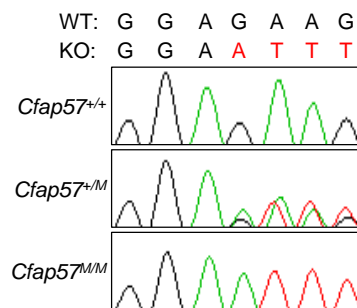
A



B

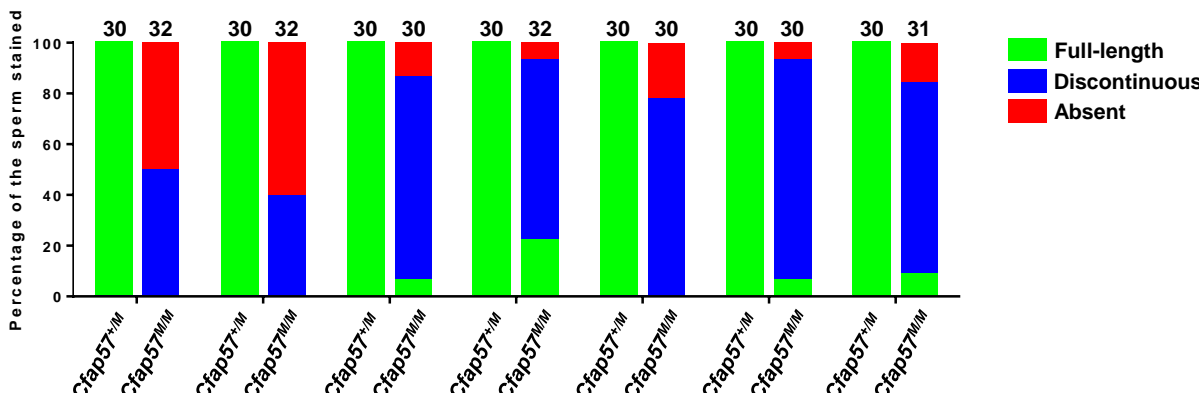
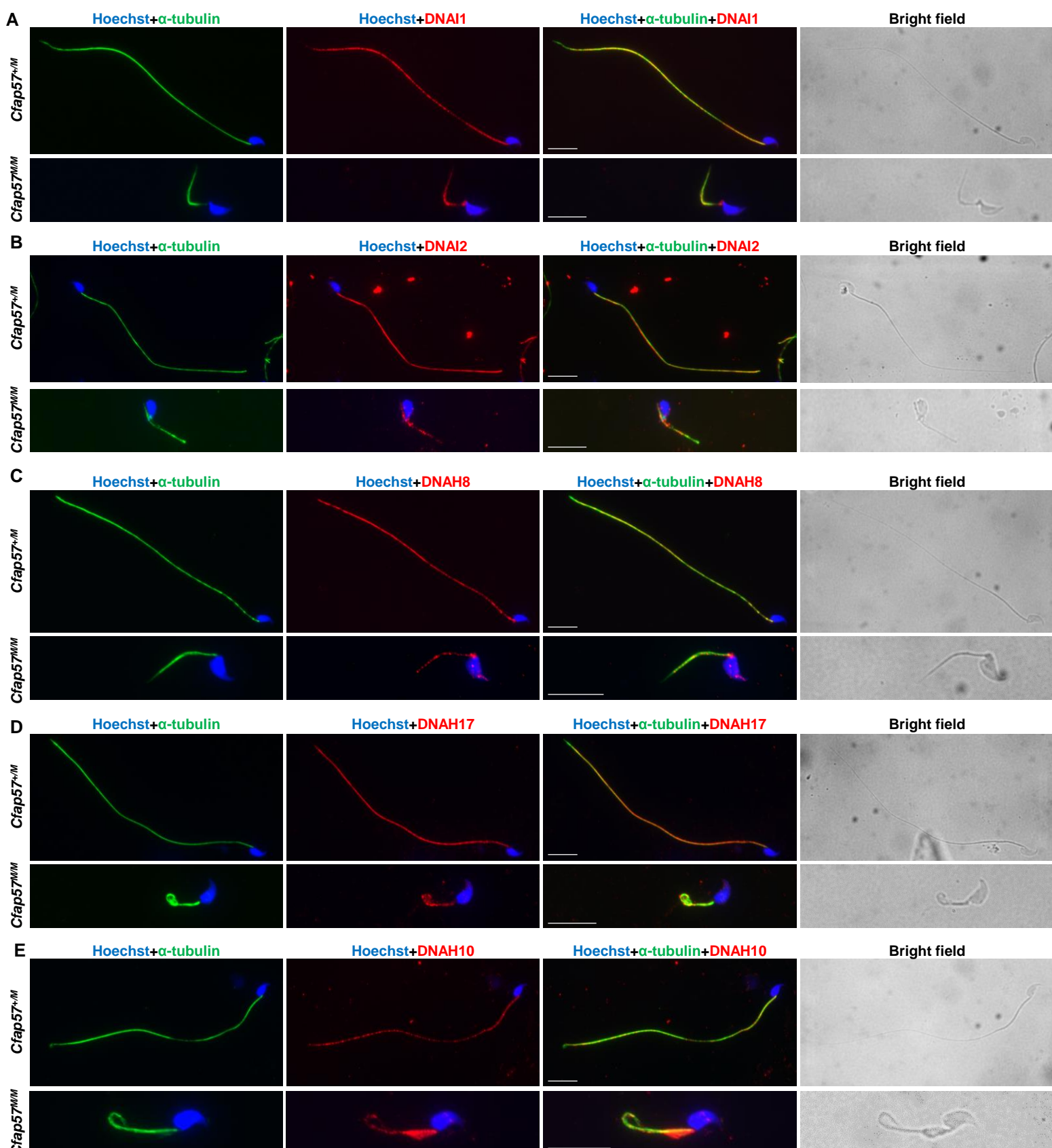


C



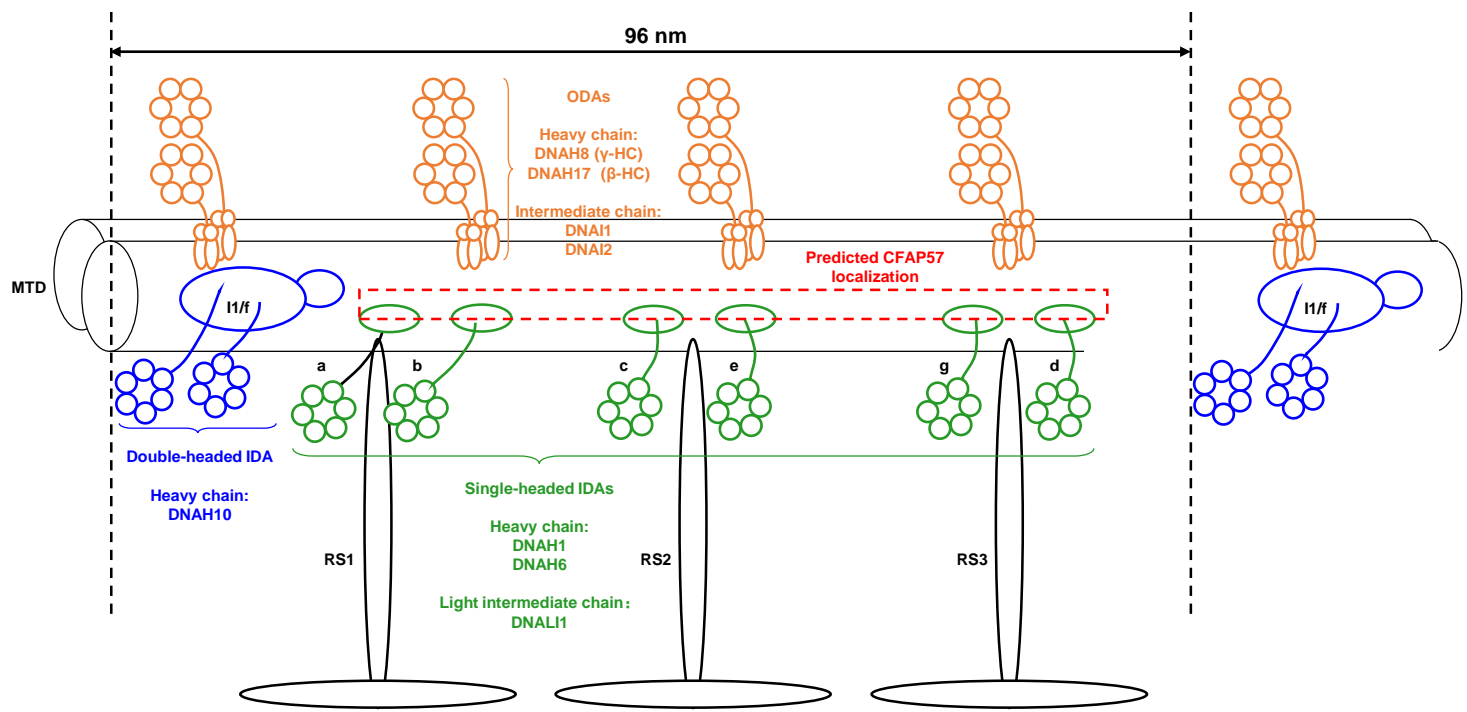
Supplementary Figure 5. *Cfap57* mutant mice were generated by CRISPR/Cas9. (A) Schematic illustrating construction of the mouse model (*Cfap57*^{MM}). (B) PAGE results showing the 7 bp deletion in *Cfap57*^{MM} mice. (C) Sanger sequencing results of *Cfap57*^{+/+}, *Cfap57*^{+/M} and *Cfap57*^{MM} mice.

Supplementary Figure 6



Supplementary Figure 6. ODA and double-headed IDA proteins still exist but show abnormal signals in sperm from *Cfap57^{MM}* mice. (A-E) Representative images of spermatozoa from *Cfap57^{+/M}* and *Cfap57^{MM}* mice co-stained with anti- α -Tubulin and anti-DNAI1 antibodies (A), anti-DNAI2 antibodies (B), anti-DNAH8 antibodies (C), anti-DNAH17 antibodies (D), or anti-DNAH10 antibodies (E). Scale bars represent 10 μ m. (F) Percentage of spermatozoa with full-length, discontinuous or absolutely absent signals of the stained antibodies. At least 30 sperm were analyzed after stained for each antibody.

Supplementary Figure 7



Supplementary Figure 7. Diagram for the localizations of proteins used as ODA/IDA markers. ODAs are drawn in orange, double-headed IDAs are drawn in blue and the single-headed IDAs are drawn in green. The red rectangle represents the predicted localization of CFAP57, which is connected to a subset of single-headed IDAs but not double-headed IDAs or ODAs.

IDA, inner dynein arm. ODA, outer dynein arm. MTD, microtubules doublet. RS, radial spoke.